Imperial College London

Imperial College London

Department of Aeronautics

Semi-Empirical Optimisation of the Shape of a Surface Reducing Turbulent Skin Friction

Author:
Herman (Hon Man) Mak

Supervisor:
Prof. Sergei Chernyshenko

Submitted in partial fulfilment of the requirements for the degree of

MSc Advanced Aeronautical Engineering

September, 2021

Abstract

Your abstract goes here. The abstract is a very brief summary of the dissertation's contents. It should be about half a page long. Somebody unfamiliar with your project should have a good idea of what it's about having read the abstract alone and will know whether it will be of interest to them.

Acknowledgements

It is usual to thank those individuals who have provided particularly useful assistance, technical or otherwise, during your project.

Contents

List of Figures

Acronyms

BL boundary layer.

CFD computational fluid dynamics.

DNS direct numerical simulation.

DR drag reduction.

ODE ordinary differential equation.

PDE partial differential equation.

SSL spatial Stokes layer.

TBL turbulent boundary layer.

TRL technology readiness level.

TSL temporal Stokes layer.

WW wavy wall.

Notation

A_g^+ riblet groove area in wall units.

A oscillation amplitude of spanwise wall velocity W_w.

h channel half height.

k wavenumber $k = \frac{2\pi}{\lambda}$ (any subscript denotes direction).

p pressure field.

$\boldsymbol{Re}$ Reynolds number, and is equal to $\frac{UL}{\nu}$, a characteristic velocity U multiplied by a characteristic length L divided by kinematic viscosity ν.

$\boldsymbol{Re}_\tau$ friction Reynolds number, defined using friction velocity u_τ and channel half height h as the characteristic velocity and length respectively.

s denoting the spatial Stokes layer (SSL) flow.

t time.

T oscillation period.

$\mathbf{u}'$ fluctuating velocity vector with components (u', v', w').

$\mathbf{U}$ velocity vector with components (U, V, W), the triple decomposition thereof is $\mathbf{U} = \overline{\mathbf{U}} + \tilde{\mathbf{u}} + \mathbf{u}'$.

U x component of velocity (similarly V, W are the y, z components of velocity respectively).

$\overline{\mathbf{U}}$ mean velocity vector with components $(\overline{U}, \overline{V}, \overline{W})$.

$\tilde{\mathbf{u}}$ phase averaged velocity vector with components $(\tilde{u}, \tilde{v}, \tilde{w})$.

$\breve{u}^+$ part of phase average velocity in the x direction dependent on $\breve{y}^+$.

$\hat{U}$ amplitude of the phase average oscillation in the x direction $\tilde{U}$.

u_τ friction wall velocity; it is equal to $\sqrt{\frac{\tau_w}{\rho}}$.

$\breve{w}^+$ part of phase average velocity in the z direction dependent on $\breve{y}^+$.

$\hat{W}$ amplitude of the phase average oscillation in the z direction $\tilde{W}$.

ww denoting the oblique wavy wall (WW) flow.

W_w spanwise wall velocity.

$\breve{y}^+$ equal to $(k_x^+)^{-1/3}\, y^+$.

0 denoting the reference channel flow.

λ wavelength (any subscript denotes direction).

μ dynamic viscosity.

ν kinematic viscosity, defined as the ratio between dynamic viscosity and density $\frac{\mu}{\rho}$.

ϕ phase along a wave.

Φ dissipation rate per unit area.

ρ fluid density.

τ_w wall shear stress.

Chapter 1

Introduction

1.1 Motivation

Whether it be water in a pipeline, or an aircraft soaring through the skies, every fluid passing by a solid and every solid passing through a fluid will experience drag. The ever pressing need to reduce our impact on the environment requires us to reduce our energy used to combat unwanted drag, which also has the added benefit of reducing costs via increased efficiency. This is especially true in the transportation sector, which accounts for 24% of total global emissions in 2019 according to the IEA, although growth has been limited to only 0.5% per year compared to an average increase of 1.9% annually since 2000 owing to efficiency improvements [1].

The search for these efficiency improvements includes research towards drag reduction (DR) via flow control – that is manipulating the flow characteristics in such a way that somehow produces less overall drag. In fact, Ludwig Prandtl, who revolutionised the study of fluid mechanics with the introduction of the turbulent boundary layer (TBL), pioneered modern flow control as early as 1904, where he demonstrated that suction at the surface of a cylinder delays boundary layer (BL) separation and therefore decreases drag [2, 3]. Indeed, DR is a major focus of research in commercial aviation. In the context of aviation, a 1% reduction in drag corresponds to a 0.75% reduction in fuel and as a result CO_2 emissions [4]. In fact, [4] states that based on estimates on travel demand in 2030, a 1% reduction will constitute a 9 million tonnes reduction in CO_2 emissions.

In transport applications, and in particular aviation, the flows are at high Reynolds numbers Re, this means the regimes we are dealing with are often turbulent. Moreover, especially in aviation (with the exception of cases where supersonic effects dominate), viscous drag generated in the near-wall BL region constitutes a major component of total drag [5]. These two factors combined mean that “flow control methodology targeting the TBL is the most obvious option to achieve a significant skin-friction-drag reduction and ultimately to reduce emissions" [5].

Flow control is separated into two distinct groups, active and passive control. Active flow control requires an input in energy to affect the flow via the use of actuators, whereas passive

flow control does not. Examples of active control include opposition control [6, 7], spanwise-wall oscillation [8–10], and the aforementioned BL separation control [3]; the former is closed-loop and reacts to sensor inputs from the environment, whereas the latter two can be either open-loop with predetermined control patterns or reactive (feedback/feed-forward systems). The actuators used to perform active flow control can range from zero-net-mass-flux jets [11], to dielectric-barrier-discharge plasma actuators [12], to fluid injection (blowing) and sucking [13], to the ingenious moving surface using "pneumatically actuated compliant structure based on the kagome lattice geometry" [14]. Whereas, examples of passive control include vortex generators [15], discontinuities/notches/fences in the leading/rear edges of a wing [15], compliant surfaces [16], porous coatings [17], superhydrophobic surfaces [18], and a very well studied control technique known as riblets [19–21].

As aforementioned, active flow control allows for reactive responses which can increase the effectiveness of control techniques. Moreover, even open-loop flow control can achieve higher viscous drag reduction than passive control techniques without the need for sensors required for reactive flow control. However, this comes at a cost of the extra energy expended to modify the flow and the difficulty and innovation needed to design actuators. This can clearly be seen in the case of spanwise-wall oscillation where the wall moves as prescribed by a streamwise travelling wave, which, after accounting for the power spent to oscillate the fluid, has a net power saving of around 26% despite a drag reduction of $> 35\%$ for those conditions [22]. Moreover, in order to emulate a in-plane wall motion in real life, the aforementioned compliant structure from [14] had to be created and trialled in laboratory conditions, and then made at scale and maintained if it were to be used on real-world flows.

On the other hand, passive flow control in necessarily open-loop, and may have decreased performance in comparison to active flow control. However, it does not require actuators and the maintenance thereof. Riblets, for example, "are small surface protrusions aligned with the direction of the flow, which confer an anisotropic roughness to a surface" [21] and can be seen in Figure 1.1. Experiments show that under moderate adverse pressure gradient (i.e. where the pressure increases along the direction of the flow) a 13% skin friction reduction is achievable, compared to 6% reduction in a zero-pressure-gradient BL [23]. Although less efficient compared to active control, due to its relatively simple design, its technology readiness level (TRL) is higher than most other flow control techniques. In fact it has been trialled in scale model aircraft tests in transonic Mach numbers [24], real aircraft tests, and even in commercial service for several years by Cathay Pacific on an Airbus A340 where 30% of the wetted surface was covered with riblets [25]. Based on a flight test on an Airbus A320, in transonic Mach number ranges, an A320 with 70% of the wetted surface covered by riblets could have a drag reduction of about 2% [26]. However, the optimal grove cross section was found to have an optimum at $\left(A_g^+\right)^{1/2} \approx 11$, where the $+$ superscript denotes non-dimensionalisation by wall units (see

Therefore, researchers have begun to explore other ways to use passive flow control for turbulent DR. The oblique wavy wall (WW) was first proposed by Chernyshenko [28] in 2013 to

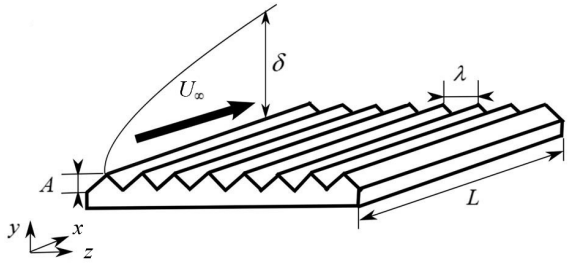

Figure 1.1: A schematic of triangular riblets; the most commonly researched riblets. Figure modified from [27].

emulate the motions of in-plane spanwise wall oscillations in hopes that there will be a net energy decrease. We will devote the rest of this report discussing the merits of this curious passive flow control method.

1.2 Literature Review

1.2.1 The Spatial Stokes Layer (SSL)

Description

The Stokes layer is one of the few known exact solutions to the Navier-Stokes equation describing the motion of a viscous fluid as a function of the wall normal coordinate y, whereby the infinitely long wall is located at the bottom at $y = 0$ and oscillating harmonically in its own plane [29]. It turns out that the resulting oscillation in the fluid is only of significant magnitude very close to the wall in a so-called "Stokes layer" and is significantly damped outside of the said-layer.

Jung et al. [8] were the first to suggest using a wall oscillating in the spanwise direction to reduce skin friction in 1992, exploiting the above phenomenon to obtain a maximum drag reduction of 40% at a non-dimensional period of $T^+ = 100$ using direct numerical simulation (DNS), a computational fluid dynamics (CFD) method [30]. The + superscript denotes non-dimensionalisation by wall units, which is based upon the wall friction velocity $u_\tau = \sqrt{\frac{\tau_w}{\rho}}$, along with the kinematic viscosity $\nu = \frac{\mu}{\rho}$, where τ_w is the wall shear stress of the fluid flow, ρ is the density of the fluid, and μ is the dynamic viscosity of the fluid flow. The spanwise velocity of the wall is given by

$$W_w = A \sin\left(\frac{2\pi}{T} t\right), \tag{1.1}$$

where A and T denotes the oscillation amplitude and period, and t denotes time. Moreover, when only one of the channel walls were oscillating, "the reduction in turbulence activity was observed only near the oscillating wall, while the flow at the other wall remained fully turbulent" [8]. When phase averaged this coincides with the Stokes layer with temporal forcing [10], we will therefore name it temporal Stokes layer (TSL). Dhanak and Si [31] observed that the duration of sweep events were reduced by 47% and their strength reduced by 23%, suggesting that the skin-friction

reduction is a result of the “attenuation in the formation of streamwise streaks [30].

As this is a form of active flow control, despite significant drag reductions, significant energy must also be expended to overcome the extra shear stress to create the spanwise motion of the fluid [10]. Baron and Quadrio [32] was the first to consider the net energy savings from spanwise wall oscillation, and it is now accepted that the net energy savings is 10% [10, 30]. However, this technique requires moving parts and therefore requires actuators, which is hard to implement in practical applications especially in transport applications.

Viotti, Quadrio, and Luchini [10] sought to extend the TSL from a time-dependent forcing to a stationary, spatial forcing, which potentially allows an extension into passive solutions which can emulate the oscillation varying over space instead of time (such as the WW). (——————————————————————————————————— kim and hussain———————————???) Letting x be the streamwise coordinate, y the wall-normal coordinate, and z the spanwise coordinate, the spatial forcing law can be seen in Figure 1.2, and is given by

$$W_w = A \sin\left(\frac{2\pi}{\lambda_x} x\right), \tag{1.2}$$

where A and λ_x denotes the forcing amplitude and the forcing wavelength in the x direction respectively. We will call this flow the spatial Stokes layer (SSL).

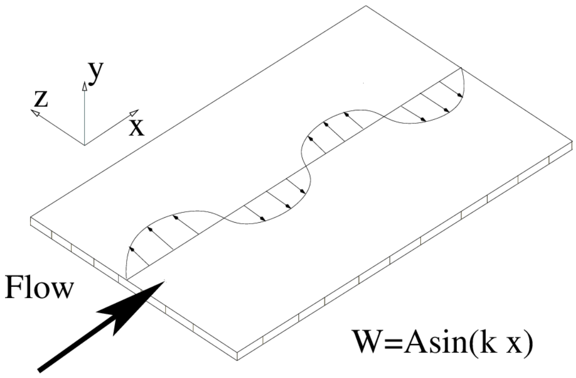

Figure 1.2: Schematic of spanwise wall forcing from [10].

Solving for Velocity

We will now analyse SSL flow analytically following Chernyshenko [28], who ultimately derives their analysis from Viotti, Quadrio, and Luchini [10]. We begin by solving for the velocity profile of SSL flow by first defining the triple decomposition of velocity as follows

$$\mathbf{U} = \overline{\mathbf{U}} + \tilde{\mathbf{u}} + \mathbf{u}', \tag{1.3}$$

where $\overline{\mathbf{U}}$ is the velocity averaged over time, and space in the x and z direction, $\tilde{\mathbf{u}}$ is the phase averaged velocity, and $\mathbf{u}'$ is the remaining stochastic turbulent part of the velocity. Unlike the traditional Reynolds decomposition, we have an extra phase dependent term, which is useful for periodic flows such as SSL flow. We can adapt the definition given in [33] to our case and define

for some phase angle $\phi_0 = \phi\left(x_0 + m\lambda_x, z_0 + n\lambda_z\right)$,

$$\tilde{\mathbf{u}}\left(y, \phi_0\right) \equiv \lim_{M\to\infty} \lim_{N\to\infty} \frac{1}{M}\frac{1}{N} \sum_{m=1}^{M} \sum_{n=1}^{N} \mathbf{U}\left(x_0 + n\lambda_x, y, z_0 + m\lambda_z\right) - \overline{\mathbf{U}}(y). \tag{1.4}$$

By including this average, we recognise that there will be periodicity in the x component of the flow velocity; we also include periodicity in the z component of the flow velocity since it will be useful for the WW flow, and doesn't affect the definition for the SSL flow, whose phase average has no z dependence and therefore $\tilde{w} = 0$.

With that definition, we can now solve for the phase averaged velocity of the SSL flow. By linearising the BL equations in the wall units of the flow around a linear profile, we ignore the stochastic fluctuations $\mathbf{u}'$ and let $\overline{\mathbf{U}}^+ = (y^+, 0, 0)$. Moreover, SSL is time invariant. Thus, by analysing the order of various values as in [29], and taking $Re \to \infty$, we get

$$y^+ \frac{\partial \tilde{u}^+}{\partial x^+} + \tilde{v}^+ = -\frac{\partial p^+}{\partial x^+} + \frac{\partial^2 \tilde{u}^+}{\partial \left(y^+\right)^2} \tag{1.5}$$

$$0 = -\frac{\partial p^+}{\partial y^+} \tag{1.6}$$

$$y^+ \frac{\partial \tilde{w}^+}{\partial x^+} = -\frac{\partial p^+}{\partial z^+} + \frac{\partial^2 \tilde{w}^+}{\partial \left(y^+\right)^2} \tag{1.7}$$

$$0 = \frac{\partial \tilde{u}^+}{\partial x^+} + \frac{\partial \tilde{v}^+}{\partial y^+} + \frac{\partial \tilde{w}^+}{\partial z^+}, \tag{1.8}$$

where p^+ is the non-dimensionalised pressure field. These are the general BL equations (also known as *Prandtl BL equations*) when linearised around a linear mean profile (i.e. where we let $\overline{U}^+ = (y^+, 0, 0)$).

(————————————————Comparison between laminar and turbulent mean fields: Fig 3 Viotti————————————————)

At the wall, we have $\tilde{u}_{\mathrm{s}}^{+\mathrm{s}}|_{y^{+\mathrm{s}}=0} = \tilde{v}_{\mathrm{s}}^{+\mathrm{s}}|_{y^{+\mathrm{s}}=0} = 0$, and $\tilde{w}_{\mathrm{s}}^{+\mathrm{s}}|_{y^{+\mathrm{s}}=0} = \hat{W}^{+\mathrm{s}} e^{ik_x^{+\mathrm{s}} x^{+\mathrm{s}}}$, where $\hat{W}_{\mathrm{s}}^{+\mathrm{s}} = A^{+\mathrm{s}}$ is the wall oscillation amplitude, $k_x^{+\mathrm{s}} = \frac{2\pi}{\lambda_x^{+\mathrm{s}}}$ is the non-dimensional wavenumber, i is the imaginary unit, the subscript s denotes that the variable is related to SSL flow, and the superscript +s denotes non-dimensionalisation by the friction velocity specific to the SSL flow $u_{\tau,\mathrm{s}} = \sqrt{\frac{\tau_{w,\mathrm{s}}}{\rho}}$, where $\tau_{w,\mathrm{s}}$ is the time, space, and phase averaged wall shear stress of the SSL flow. Although strictly speaking $\tilde{w}_{\mathrm{s}}^{+\mathrm{s}}|_{y=0}$ is only the real part of the exponential function (as well as any other phase averaged terms that we prescribe the exponential function for the rest of this report), however analysis is much more easily done using the exponential function and only taking the real part thereof at the very end. Moreover, since the wall is flat, we expect the pressure gradient in all directions to be zero. We also only expect the spanwise periodic fluctuations to be non-zero, therefore $\tilde{u}_{\mathrm{s}} = \tilde{v}_{\mathrm{s}} = 0$. This means that to solve for $\tilde{w}^{+\mathrm{s}}$ we only need Equation (1.7).

Finally, we expect the spanwise velocity to vary not only in x (due to the x dependence of the prescribed spanwise wall forcing), but also in y as the Stokes layer decreases in strength away from the wall. Therefore, we get

$$\tilde{w}^{+\mathrm{s}}\left(x^{+\mathrm{s}}, \breve{y}^{+\mathrm{s}}\right) = \hat{W}_{\mathrm{s}}^{+\mathrm{s}} \breve{w}_{\mathrm{s}}^{+\mathrm{s}} e^{ik_x^{+\mathrm{s}} x^{+\mathrm{s}}}, \tag{1.9}$$

where we define $y^+ = (k_x^+)^{-1/3}\,\check{y}^+$ in order to simplify or equations later, and $\check{w}_\mathrm{s}^{+\mathrm{s}} = \check{w}_\mathrm{s}^{+\mathrm{s}}(\check{y}^{+\mathrm{s}})$ as the only part of $\tilde{w}^{+\mathrm{s}}$ dependent on $\check{y}^{+\mathrm{s}}$. Therefore Equation (1.7) becomes

$$\begin{aligned}\left(k_x^{+\mathrm{s}}\right)^{-1/3}\check{y}^{+\mathrm{s}}\frac{\partial}{\partial x^{+\mathrm{s}}}\left(\hat{W}^{+\mathrm{s}}\check{w}_\mathrm{s}^{+\mathrm{s}}e^{ik_x^{+\mathrm{s}}x^{+\mathrm{s}}}\right) &= \frac{\partial^2}{\partial\left((k_x^{+\mathrm{s}})^{-1/3}\check{y}\right)^2}\left(\hat{W}^{+\mathrm{s}}\check{w}_\mathrm{s}^{+\mathrm{s}}e^{ik_x^{+\mathrm{s}}x^{+\mathrm{s}}}\right)\\ i\check{y}^{+\mathrm{s}}\check{w}_\mathrm{s}^{+\mathrm{s}} &= \frac{\mathrm{d}^2\check{w}_\mathrm{s}^{+\mathrm{s}}}{\mathrm{d}(\check{y}^{+\mathrm{s}})^2}.\end{aligned} \tag{1.10}$$

We can see that we can solve for $\check{w}_\mathrm{s}^{+\mathrm{s}}$ with only an ordinary differential equation (ODE). We know that at the wall $\check{w}_\mathrm{s}^{+\mathrm{s}}|_{\check{y}^{+\mathrm{s}}=0} = 1$, and since this is a Stokes layer, we want $\check{w}_\mathrm{s}^{+\mathrm{s}} \to 0$ as $\check{y}^{+\mathrm{s}} \to \infty$. This ODE can either be solved numerically or be described by an Airy function (denoted $\mathrm{Ai}(\cdot)$) as follows,

$$\check{w}_\mathrm{s}^{+\mathrm{s}}(\check{y}^{+\mathrm{s}}) = \frac{\mathrm{Ai}\left(-i\check{y}^{+\mathrm{s}}e^{-\frac{4}{3}i\pi}\right)}{\mathrm{Ai}(0)}, \tag{1.11}$$

which gives

$$w_\mathrm{s}^{+\mathrm{s}} = \mathrm{Re}\left[\hat{W}_\mathrm{s}^{+\mathrm{s}}e^{ik_x^{+\mathrm{s}}x}\frac{\mathrm{Ai}\left(-i\check{y}^{+\mathrm{s}}e^{-\frac{4}{3}i\pi}\right)}{\mathrm{Ai}(0)}\right]. \tag{1.12}$$

Net Power Definition

Our ultimate goal is of course to find how much energy we might be able to save using SSL. We will calculate the net power saved by having SSL in both the top and bottom wall of an infinite flat channel (which was what was done in Viotti, Quadrio, and Luchini [10] such that comparisons can be made with DNS, which requires a finite domain), compared with a reference channel flow with no movement. We will denote variables relating to the reference flow with a subscript 0, and similar to the SSL flow, we will denote non-dimensionalisation by the wall units of the reference flow with the superscript $+0$.

To find this elusive net power saving, we start with conservation of energy in the channel. Thus,

$$P_\mathrm{in}^+ = P_\mathrm{out}^+, \tag{1.13}$$

where P denotes power per unit area. We know for SSL, P_in includes some sort of external pump that powers the flow against drag (which we hope is reduced from the reference flow), as well as an actuator or motor which drives the oscillatory in-plane wall motion. Whereas for the reference flow P_in does not have the latter. On the other hand, the P_out of the system is purely through losses in heat, which comes from dissipation in the fluid, which, per unit area, is given by

$$\Phi^+ = \int_0^\infty \overline{\left(\frac{\mathrm{d}\mathbf{U}^+}{\mathrm{d}y^+}\right)^2}\,\mathrm{d}y^+\,, \tag{1.14}$$

for one wall, where the overbar denotes conducting averaging and phase averaging in time and space in the x, z directions. Despite this being channel flow, we integrate to infinity instead of the channel half height as the analysis is easier to deal with and it is presumed that $\frac{\mathrm{d}\mathbf{U}^+}{\mathrm{d}y^+} \to 0$ quickly as $y^+ \to \infty$ outside the boundary layer. Using the incredibly useful triple decomposition,

the dissipation per unit area becomes

$$\Phi^+ = \int_0^\infty \overline{\left(\frac{\mathrm{d}}{\mathrm{d}y^+}\left(\overline{\mathbf{U}}^+ + \tilde{\mathbf{u}}^+ + \mathbf{u}'\right)\right)^2}\,\mathrm{d}y^+ \tag{1.15}$$

$$= \int_0^\infty \left[\overline{\left(\frac{\mathrm{d}\overline{\mathbf{U}}}{\mathrm{d}y^+}\right)^2} + \overline{\left(\frac{\mathrm{d}\tilde{\mathbf{u}}}{\mathrm{d}y^+}\right)^2} + \overline{\left(\frac{\mathrm{d}\mathbf{u}'}{\mathrm{d}y^+}\right)^2} + 2\left(\overline{\frac{\mathrm{d}\overline{\mathbf{U}}}{\mathrm{d}y^+}\frac{\mathrm{d}\tilde{\mathbf{u}}}{\mathrm{d}y^+}} + \overline{\frac{\mathrm{d}\overline{\mathbf{U}}}{\mathrm{d}y^+}\frac{\mathrm{d}\mathbf{u}'}{\mathrm{d}y^+}} + \overline{\frac{\mathrm{d}\tilde{\mathbf{u}}}{\mathrm{d}y^+}\frac{\mathrm{d}\mathbf{u}'}{\mathrm{d}y^+}}\right)^{0} \right] \mathrm{d}y^+ \tag{1.16}$$

$$= \int_0^\infty \overline{\left(\frac{\mathrm{d}\overline{\mathbf{U}}}{\mathrm{d}y^+}\right)^2}\,\mathrm{d}y^+ + \int_0^\infty \overline{\left(\frac{\mathrm{d}\tilde{\mathbf{u}}}{\mathrm{d}y^+}\right)^2}\,\mathrm{d}y^+ + \int_0^\infty \overline{\left(\frac{\mathrm{d}\mathbf{u}'}{\mathrm{d}y^+}\right)^2}\,\mathrm{d}y^+ . \tag{1.17}$$

Wonderfully, the cross terms inside the final brackets of 1.16 all go to zero since the overbar for dissipation involves both the mean averaging and phase averaging, and since $\overline{\overline{a}b} = \overline{a}\,\overline{b}$ for any a, b, and the average of a fluctuating quantity is zero. Moreover, since the flows being considered throughout the rest of the report have a mean velocity in the y or z direction, nor will they have a phase averaged velocity in the y direction we can then reduce the dissipation further to

$$\Phi^+ = \int_0^\infty \overline{\left(\frac{\mathrm{d}\overline{U}}{\mathrm{d}y^+}\right)^2}\,\mathrm{d}y^+ + \int_0^\infty \overline{\left(\frac{\mathrm{d}}{\mathrm{d}y^+}(\tilde{u},\tilde{w},0)\right)^2}\,\mathrm{d}y^+ + \int_0^\infty \overline{\left(\frac{\mathrm{d}\mathbf{u}'}{\mathrm{d}y^+}\right)^2}\,\mathrm{d}y^+ \tag{1.18}$$

$$= \int_0^\infty \overline{\left(\frac{\mathrm{d}\overline{U}}{\mathrm{d}y^+}\right)^2}\,\mathrm{d}y^+ + \int_0^\infty \overline{\left(\frac{\mathrm{d}\tilde{u}}{\mathrm{d}y^+}\right)^2}\,\mathrm{d}y^+ + \int_0^\infty \overline{\left(\frac{\mathrm{d}\tilde{w}}{\mathrm{d}y^+}\right)^2}\,\mathrm{d}y^+ + \int_0^\infty \overline{\left(\frac{\mathrm{d}\mathbf{u}'}{\mathrm{d}y^+}\right)^2}\,\mathrm{d}y^+ \tag{1.19}$$

$$\equiv \Phi^+_{\overline{U}} + \Phi^+_{\tilde{u}} + \Phi^+_{\tilde{w}} + \Phi^+_{\mathbf{u}'}. \tag{1.20}$$

For the reference flow $\Phi^{+0}_0 = \Phi^{+0}_{\overline{U},0} + \Phi^{+0}_{\mathbf{u}',0}$, whereas for the SSL flow $\Phi^{+\mathrm{s}}_{\mathrm{s}} = \Phi^{+\mathrm{s}}_{\overline{U},\mathrm{s}} + \Phi^{+\mathrm{s}}_{\tilde{w},\mathrm{s}} + \Phi^{+\mathrm{s}}_{\mathbf{u}',\mathrm{s}}$. Therefore we can call the $\overline{U}$ and $\mathbf{u}'$ portions of dissipation drag, and the extra $\tilde{w}$ portion of dissipation an extra required portion for the SSL flow.

Let us now define the net power reduction of the SSL channel flow as a percentage of the reference channel flow as follows,

$$P_{\mathrm{net,s}} \equiv 100\%\frac{2\Phi^{+0}_0 - 2\Phi^{+0}_{\mathrm{s}}}{2\Phi^{+0}_0} \tag{1.21}$$

$$= 100\%\frac{\Phi^{+0}_{\overline{U},0} + \Phi^{+0}_{\mathbf{u}',0} - \left(\Phi^{+0}_{\overline{U},\mathrm{s}} + \Phi^{+0}_{\tilde{w},\mathrm{s}} + \Phi^{+0}_{\mathbf{u}',\mathrm{s}}\right)}{\Phi^{+0}_0} \tag{1.22}$$

$$= 100\%\frac{\left(\Phi^{+0}_{\overline{U},0} - \Phi^{+0}_{\overline{U},\mathrm{s}}\right) + \left(\Phi^{+0}_{\mathbf{u}',0} - \Phi^{+0}_{\mathbf{u}',\mathrm{s}}\right)}{\Phi^{+0}_0} + 100\%\frac{\left(0 - \Phi^{+0}_{\tilde{w},\mathrm{s}}\right)}{\Phi^{+0}_0} \tag{1.23}$$

$$= 100\%\frac{\Delta\Phi^{+0}_{\overline{U},\mathrm{s}} + \Delta\Phi^{+0}_{\mathbf{u}',\mathrm{s}}}{\Phi^{+0}_0} + 100\%\frac{\Delta\Phi^{+0}_{\tilde{w},\mathrm{s}}}{\Phi^{+0}_0} \tag{1.24}$$

$$\equiv P_{\mathrm{sav,s}} + P_{\mathrm{req,s}}, \tag{1.25}$$

where $P_{\mathrm{sav,s}}$ and $P_{\mathrm{req,s}}$ are the resulting power saved due to drag reduction and power required to maintain forcing to conteract spanwise velocity gradients respectively; both are expressed as a percentage of the power required to drive the reference flow. The definition here is numerically equivalent to that of Viotti, Quadrio, and Luchini [10], which defines them as a function of dimensional units.

Power Saved from SSL Wall Forcing

$P_{\text{sav,s}}$ was obtained from DNS results from Viotti, Quadrio, and Luchini [10], which was again conducted at $Re_\tau = 200$ using different forcing wavelengths λ_x^{+0}, and forcing amplitudes $\hat{W}_\text{s}^{+0} = 1, 2, 6, 12$. Chernyshenko [28] only used data up to $\lambda_x^{+0} < 3000$, which was digitised via the webapp *WebPlotDigitizer*, and fitted $P_{\text{sav,s}}$ at each $\hat{W}_\text{s}^{+0}$ on a degree 5 polynomial of λ_x^{+0}, i.e.

$$P_{\text{sav,s}} = f\left(\lambda_x^{+0}, \hat{W}_\text{s}^{+0}\right) \tag{1.26}$$

$$= c_{0,\hat{W}_\text{s}^{+0}} + c_{1,\hat{W}_\text{s}^{+0}}\lambda_x^{+0} + c_{2,\hat{W}_\text{s}^{+0}}\left(\lambda_x^{+0}\right)^2 + c_{3,\hat{W}_\text{s}^{+0}}\left(\lambda_x^{+0}\right)^3 + c_{4,\hat{W}_\text{s}^{+0}}\left(\lambda_x^{+0}\right)^4 + c_{5,\hat{W}_\text{s}^{+0}}\left(\lambda_x^{+0}\right)^5, \tag{1.27}$$

where the coefficients are given in Table 1.1. The data and curvefits thereof are shown in Figure1.3

$\hat{W}_\text{s}^{+0}$	c_0	c_1	c_2	c_3	c_4	c_5
1	1.135	0.002 929	-1.205×10^{-6}	1.447×10^{-10}	-1.047×10^{-13}	2.609×10^{-17}
2	−1.856	0.039 54	-5.285×10^{-5}	3.498×10^{-8}	-1.127×10^{-11}	1.328×10^{-15}
6	15.25	0.048 88	-4.441×10^{-5}	1.628×10^{-8}	-2.845×10^{-12}	1.938×10^{-16}
12	27.90	0.038 24	-2.810×10^{-5}	8.015×10^{-9}	-1.082×10^{-12}	5.535×10^{-17}

Table 1.1: Coefficients of curvefits of $P_{\text{sav,s}}$ data from DNS for different forcing wavelength λ_x^{+0} using different forcing amplitudes $\hat{W}_\text{s}^{+0}$ by Viotti, Quadrio, and Luchini [10]

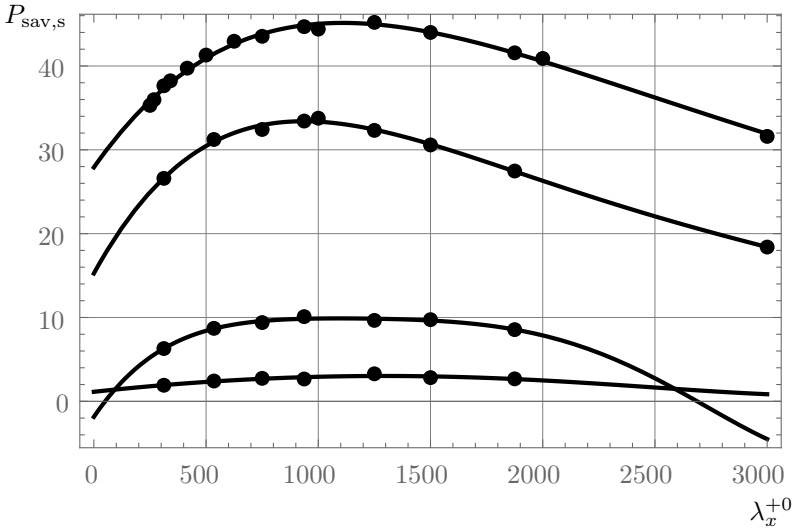

Figure 1.3: Power saved due to drag reduction in the SSL flow, $P_{\text{sav,s}}$, as a function of wall forcing wavelength λ_x^{+0}. The curvefits from Chernyshenko [28] and corresponding data from Viotti, Quadrio, and Luchini [10] are for forcing amplitudes $\hat{W}_\text{s}^{+0} = 1, 2, 6, 12$ which are in order from the bottom to top curve. The figure is slightly modified from [28].

Power Required to Drive SSL Wall Forcing

In order to find $P_{\text{req,s}}$, we begin by expressing $\Delta\Phi^{+0}_{\tilde{w},\text{s}} = -\Phi^{+0}_{\tilde{w},\text{s}}$ in the wall units of the SSL flow. This requires recognising that dissipation per unit area Φ has the units of power per unit area, which is equivalent to velocity times force per unit area. This means that Φ^{+} is non-dimensionalised with the relevant $u_\tau \tau_w$. We will use that below to get

$$\Phi^{+0}_{\tilde{w},\text{s}} = \frac{\Phi_{\tilde{w},\text{s}}}{u_{\tau,0}\tau_{w,0}} \tag{1.28}$$

$$= \frac{\Phi_{\tilde{w},\text{s}}}{u_{\tau,\text{s}}\tau_{w,\text{s}}} \frac{u_{\tau,\text{s}}\tau_{w,\text{s}}}{u_{\tau,0}\tau_{w,0}} \tag{1.29}$$

$$= \Phi^{+\text{s}}_{\tilde{w},\text{s}} \left(\frac{\tau_{w,\text{s}}}{\tau_{w,0}}\right)^{3/2}. \tag{1.30}$$

Now we will find $\Phi^{+\text{s}}_{\tilde{w},\text{s}}$ by using Equation (1.9) as follows

$$\Phi^{+\text{s}}_{\tilde{w},\text{s}} = \int_0^\infty \overline{\left(\frac{\mathrm{d}\tilde{w}^{+\text{s}}_{\text{s}}}{\mathrm{d}y^{+\text{s}}}\right)^2}\, \mathrm{d}y^{+\text{s}} \tag{1.31}$$

$$= \int_0^\infty \left(\frac{\mathrm{d}\overline{\hat{W}^{+\text{s}}_{\text{s}} \check{w}^{+\text{s}}_{\text{s}} e^{ik_x^{+\text{s}} x^{+\text{s}}}}}{\mathrm{d}\left((k_x^{+\text{s}})^{-1/3}\check{y}^{+\text{s}}\right)}\right)^2 \mathrm{d}\left(\left(k_x^{+\text{s}}\right)^{-1/3}\check{y}^{+\text{s}}\right) \tag{1.32}$$

$$= \left(\hat{W}^{+\text{s}}_{\text{s}}\right)^2 \left(k_x^{+\text{s}}\right)^{1/3} \int_0^\infty \frac{1}{2}\left(\frac{\mathrm{d}\check{w}^{+\text{s}}_{\text{s}}}{\mathrm{d}\check{y}^{+\text{s}}}\right)^2 \mathrm{d}\check{y}^{+\text{s}}. \tag{1.33}$$

Since $\check{w}^{+\text{s}}_{\text{s}}$ is a known function that we found in Equation (1.11), it is possible to evaluate the integral numerically. Chernyshenko [28] gives $\int_0^\infty \frac{1}{2}\left(\frac{\mathrm{d}\check{w}^{+\text{s}}_{\text{s}}}{\mathrm{d}\check{y}^{+\text{s}}}\right)^2 \mathrm{d}\check{y}^{+\text{s}} = 0.3157$. For the other two terms, we wish to non-dimensionalise them with $^{+0}$units similar to Equation (1.30), as that is the units that are presented in Viotti, Quadrio, and Luchini [10], whose data we will use for calculating both $P_{\text{net,s}}$ and $P_{\text{net,ww}}$. Thus,

$$k_x^{+\text{s}} = \frac{2\pi}{\lambda_x^{+\text{s}}} = \frac{2\pi}{\lambda u_{\tau,\text{s}}/\nu}\frac{u_{\tau,0}/\nu}{u_{\tau,0}/\nu} = \frac{2\pi}{\lambda_x^{+0}}\left(\frac{\tau_{w,\text{s}}}{\tau_{w,0}}\right)^{-1/2}, \tag{1.34}$$

and

$$\hat{W}^{+\text{s}}_{\text{s}} = \frac{\hat{W}_{\text{s}}}{u_{\tau,\text{s}}}\frac{u_{\tau,0}}{u_{\tau,0}} = \hat{W}^{+0}_{\text{s}}\left(\frac{\tau_{w,\text{s}}}{\tau_{w,0}}\right)^{-1/2}. \tag{1.35}$$

The ratio of wall shear stress is incredibly useful, as by the definition of $P_{\text{sav,s}}$, it is equivalent to

$$P_{\text{sav,s}} = 100\%\frac{\tau_{w,0} - \tau_{w,\text{s}}}{\tau_{w,0}} \implies \frac{\tau_{w,\text{s}}}{\tau_{w,0}} = 1 - \frac{P_{\text{sav,s}}}{100\%}. \tag{1.36}$$

Finally, we know that for the flat plate reference flow the dissipation on one side of the channel is given by $\Phi^{+0}_0 = U^{+0}_b$, where U_b is the bulk velocity (the time and space averaged velocity in the channel) [28]. Definitionally, the coefficient of friction of a flow based on the bulk velocity is given by $C_f = \frac{\tau_w}{\frac{1}{2}\rho U_b} = \frac{2u_\tau}{U_b} = \frac{2}{U^+_b}$. Therefore,

$$\Phi^{+0}_0 = U^{+0}_b = \sqrt{\frac{2}{C_{f,0}}}. \tag{1.37}$$

DNS by Viotti, Quadrio, and Luchini [10] at $Re_\tau = 200$ was in good correlation with the estimate $C_{f,0} = 0.0336 Re_\tau^{-0.273}$ given by [34], where Re_τ is the friction Reynolds number, defined using the

friction velocity u_τ and channel half height h as the characteristic velocity and length respectively. As in [10, 28], we will use this estimate. Thus, from the definition of $P_{\text{req,s}}$ in Equation (1.25), and by using Equations (1.30), (1.33), (1.34), (1.35), (1.36), and (1.37), we get

$$P_{\text{req,s}} = -100\% \frac{\Phi_{\text{s}}^{+0}}{\Phi_0^{+0}} \tag{1.38}$$

$$= -100\% \left(\hat{W}_{\text{s}}^{+0}\right)^2 \sqrt{\frac{C_{f,0}}{2}} \left(\frac{2\pi}{\lambda_x^{+\text{s}}} \left(1 - \frac{P_{\text{sav,s}}}{100\%}\right)\right)^{1/3} \int_0^\infty \frac{1}{2} \left(\frac{\mathrm{d}\check{w}_{\text{s}}^{+\text{s}}}{\mathrm{d}\check{y}^{+\text{s}}}\right)^2 \mathrm{d}\check{y}^{+\text{s}} \tag{1.39}$$

$$= -100\%(0.3157) \left(\hat{W}_{\text{s}}^{+0}\right)^2 \sqrt{\frac{C_{f,0}}{2}} \left(\frac{2\pi}{\lambda_x^{+\text{s}}} \left(1 - \frac{P_{\text{sav,s}}}{100\%}\right)\right)^{1/3}. \tag{1.40}$$

By inserting $P_{\text{sav,s}}$ from Equation (1.27) for each $\hat{W}_{\text{s}}^{+0}$ with the corresponding coefficients from Table 1.1, we will find $P_{\text{req,s}}$. We plot in Figure 1.4

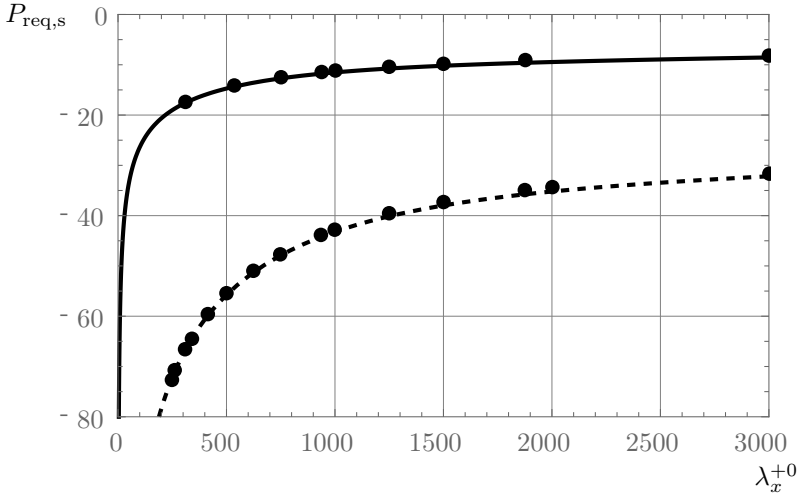

Figure 1.4: Power required to drive the forcing in the SSL flow, $P_{\text{req,s}}$, as a function of wall forcing wavelength λ_x^{+0} from Equation (1.40) at $\hat{W}_{\text{s}}^{+0} = 6$ (solid) and $\hat{W}_{\text{s}}^{+0} = 12$ (dashed) with corresponding DNS data from Viotti, Quadrio, and Luchini [10]. The figure is slightly modified from [28].

SSL Final Results

By using Equation (1.25), which says $P_{\text{net,s}} = P_{\text{sav,s}} + P_{\text{req,s}}$, the results for $\hat{W}_{\text{s}}^{+0}$ along with its corresponding DNS data are plotted in Figure 1.5. Based on these results of Viotti, Quadrio, and Luchini [10] at their parameters, it can be shown that a maximum net power decrease of 23% at $\hat{W}_{\text{s}}^{+0} = 6$ and at $\lambda_x^{+0} = 1000 - 1250$.

Other results presented by Viotti, Quadrio, and Luchini [10], include the clear modification of the near-wall turbulence compared to the reference case, with much fewer turbulent vortical structures visible based on a λ_2^{+0} quantity introduced by Jeong and Hussain [35] that they set at -0.03 that we will not discuss here. They also found a reduction of the turbulence intensity (the root-mean-square of turbulent fluctuations). Most importantly for this project, they found that, like other DR techniques (such as riblets), "[t]he DR manifests itself through the thickening of the

viscous sublayer, which results in the upward shift of the logarithmic portion of the velocity profile" [10]. This result will be explored later in this report. (————————————-section?————————————————————————————-)

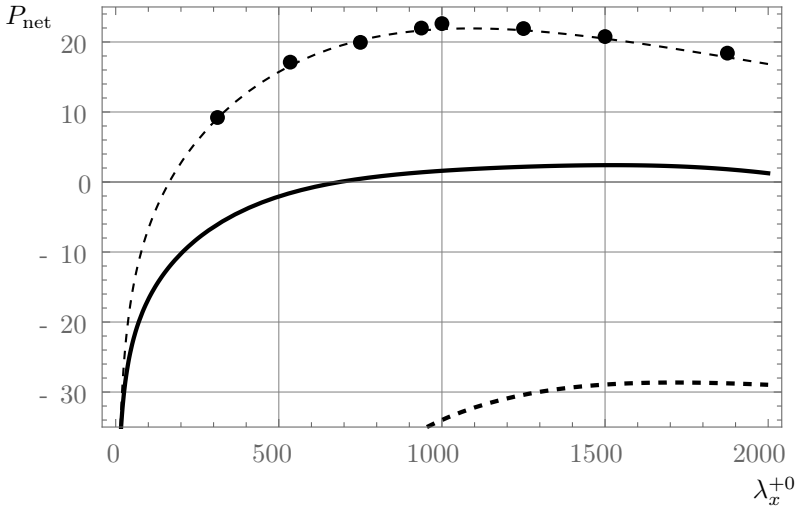

Figure 1.5: Net power reduction P_{net} as a function of wall forcing wavelength λ_x^{+0} for SSL at $\hat{W}_{\text{s}}^{+0} = 6$ (thin-dashes) corresponding DNS data from Viotti, Quadrio, and Luchini [10], and for WW at $\hat{W}_{\text{ww}}^{+0} = 2$ (solid) and at $\hat{W}_{\text{ww}}^{+0} = 6$ (thick-dashes). The figure is slightly modified from [28].

1.2.2 The Oblique Wavy Wall (WW)

Description

As mentioned in Section 1.1, TSL and SSL are active control strategy, which requires actuators. Several mechanisms are being trialed in laboratories experimentally to effect TSL or SSL such as dielectric-barrier discharge plasma actuators [36], azimuthally moving pipe walls [37], etc. However, as these actuators have low TRL, SSL was conjectured, analysed, and simulated via CFD mainly so that a passive device (most likely via wall roughness) could emulate the flow patterns to affect the TBL the same way to reduce drag. In fact, Viotti, Quadrio, and Luchini [10] mentions a patent for riblets that would oscillate sinusoidally in the streamwise direction [38]; the idea has been briefly studied although the positive effects of small amplitudes "could not be determined outside the uncertainty range", whilst the larger amplitudes actually reduce the total drag reduction due to increase in pressure drag [39]. The same authors claimed that a 1.3% drag reduction was possible [40] More research should be done on that to better evaluate its viability.

In [28] Chernyshenko proposes instead to use an undulating wavy wall (WW) placed at an oblique angle to the direction of the flow (Figure 1.6). Since this wavy wall is at an angle to the streamwise direction, it creates a spanwise pressure gradient that accelerates it towards the crests when approaching them and when leaving them. This oscillatory force that the fluid experiences generates alternating spanwise motion [41]. An visualisation of the SSL forcing and WW in Figure 1.7 shows that the spanwise oscillation caused

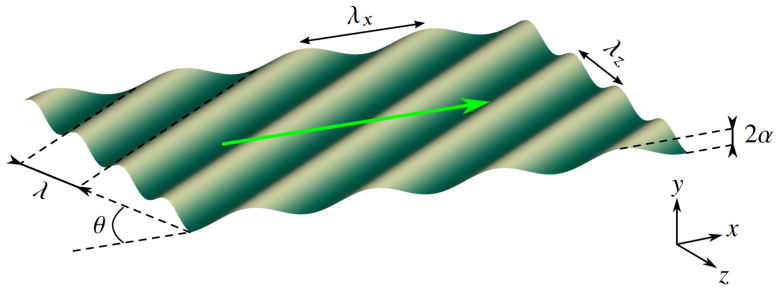

Figure 1.6: Schematic of the oblique wavy wall from [42]. The green arrow represents the flow direction, at an oblique angle θ to the wavy wall.

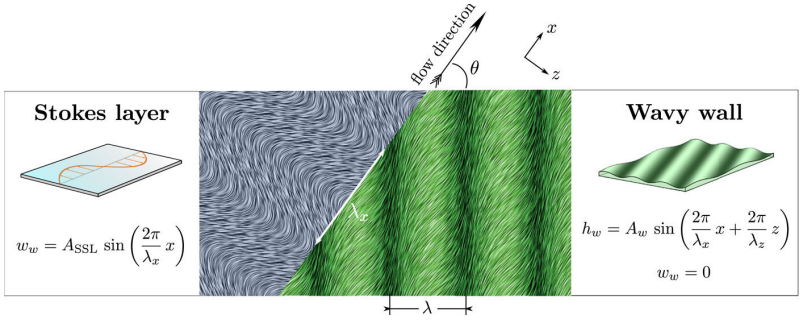

Figure 1.7: An emulation of the forcing by SSL (left) and WW (right) showing mean streaklines close to the wall, where the background is coloured according to the norm of the velocity vector.

Chapter 2

Conclusion

Code is broken

τ_w/τ_0 problem Ycross is enough to find Pnet Subject to (1) the closed system has been obtained

Wave height versus pressure

Bibliography

[1] IEA. *Transport - Improving the Sustainability of Passenger and Freight Transport*. IEA. 2021. URL: https://www.iea.org/topics/transport (visited on 14/09/2021).

[2] Mohamed Gad-el-Hak. 'Flow Control: The Future'. In: *Journal of Aircraft* 38.3 (2001), pp. 402–418. DOI: 10.2514/2.2796. URL: https://doi.org/10.2514/2.2796 (visited on 15/09/2021).

[3] Ludwig Prandtl. 'Über Flüssigkeitsbewegung bei sehr kleiner Reibung'. In: *Proceedings of the Third International Mathematical Congress*. Proceedings of the Third International Mathematical Congress. Heidelberg, 8th–13th Aug. 1904, pp. 484–491.

[4] Michael A. Leschziner, Haecheon Choi, and Kwing-So Choi. 'Flow-Control Approaches to Drag Reduction in Aerodynamics: Progress and Prospects'. In: *Philosophical Transactions of the Royal Society A: Mathematical, Physical and Engineering Sciences* 369.1940 (13th Apr. 2011), pp. 1349–1351. DOI: 10.1098/rsta.2010.0375. URL: https://doi.org/10.1098/rsta.2010.0375 (visited on 16/09/2021).

[5] Adel Abbas et al. 'Drag Reduction via Turbulent Boundary Layer Flow Control'. In: *Science China Technological Sciences* 60.9 (1st Sept. 2017), pp. 1281–1290. ISSN: 1869-1900. DOI: 10.1007/s11431-016-9013-6. URL: https://doi.org/10.1007/s11431-016-9013-6 (visited on 14/09/2021).

[6] Haecheon Choi, Parviz Moin, and John Kim. 'Active Turbulence Control for Drag Reduction in Wall-Bounded Flows'. In: *Journal of Fluid Mechanics* 262 (1994), pp. 75–110. ISSN: 0022-1120. DOI: 10.1017/S0022112094000431. URL: https://www.cambridge.org/core/article/active-turbulence-control-for-drag-reduction-in-wallbounded-flows/3075211F21E692996F66BF17D63CA649 (visited on 15/09/2021).

[7] M. Luhar, A. S. Sharma, and B. J. McKeon. 'Opposition Control within the Resolvent Analysis Framework'. In: *Journal of Fluid Mechanics* 749 (June 2014), pp. 597–626. ISSN: 0022-1120, 1469-7645. DOI: 10.1017/jfm.2014.209. URL: https://www.cambridge.org/core/journals/journal-of-fluid-mechanics/article/opposition-control-within-the-resolvent-analysis-framework/710BD53A61478AFA2DB02355FF7C4FB8 (visited on 15/09/2021).

[8] W. J. Jung, N. Mangiavacchi, and R. Akhavan. 'Suppression of Turbulence in Wall-bounded Flows by High-frequency Spanwise Oscillations'. In: *Physics of Fluids A: Fluid Dynamics* 4.8 (1st Aug. 1992), pp. 1605–1607. ISSN: 0899-8213. DOI: 10.1063/1.858381. URL: https://aip.scitation.org/doi/abs/10.1063/1.858381 (visited on 15/09/2021).

[9] Kwing-So Choi, Jean-Robert DeBisschop, and Brian R. Clayton. 'Turbulent Boundary-Layer Control by Means of Spanwise-Wall Oscillation'. In: *AIAA Journal* 36.7 (1st July 1998), pp. 1157–1163. ISSN: 0001-1452. DOI: 10.2514/2.526. URL: https://arc.aiaa.org/doi/10.2514/2.526 (visited on 15/09/2021).

[10] Claudio Viotti, Maurizio Quadrio, and Paolo Luchini. 'Streamwise Oscillation of Spanwise Velocity at the Wall of a Channel for Turbulent Drag Reduction'. In: *Physics of Fluids* 21.11 (Nov. 2009), p. 115109. ISSN: 1070-6631, 1089-7666. DOI: 10.1063/1.3266945. URL: http://aip.scitation.org/doi/10.1063/1.3266945 (visited on 15/09/2021).

[11] PanFeng Zhang, JinJun Wang, and LiHao Feng. 'Review of Zero-Net-Mass-Flux Jet and Its Application in Separation Flow Control'. In: *Science in China Series E: Technological Sciences* 51.9 (8th Aug. 2008), p. 1315. ISSN: 1862-281X. DOI: 10.1007/s11431-008-0174-x. URL: https://doi.org/10.1007/s11431-008-0174-x (visited on 15/09/2021).

[12] Jin-Jun Wang et al. 'Recent Developments in DBD Plasma Flow Control'. In: *Progress in Aerospace Sciences* 62 (1st Oct. 2013), pp. 52–78. ISSN: 0376-0421. DOI: 10.1016/j.paerosci.2013.05.003. URL: https://www.sciencedirect.com/science/article/pii/S0376042113000535 (visited on 15/09/2021).

[13] T. L. Chng et al. 'Flow Control of an Airfoil via Injection and Suction'. In: *Journal of Aircraft* 46.1 (1st Jan. 2009), pp. 291–300. DOI: 10.2514/1.38394. URL: https://arc.aiaa.org/doi/10.2514/1.38394 (visited on 15/09/2021).

[14] James Bird, Matthew Santer, and Jonathan F. Morrison. 'Experimental Control of Turbulent Boundary Layers with In-Plane Travelling Waves'. In: *Flow, Turbulence and Combustion* 100.4 (1st June 2018), pp. 1015–1035. ISSN: 1573-1987. DOI: 10.1007/s10494-018-9926-2. URL: https://doi.org/10.1007/s10494-018-9926-2 (visited on 15/09/2021).

[15] Paul K. Chang. 'CHAPTER XII - Control of Separation of Flow'. In: *Separation of Flow*. Ed. by Paul K. Chang. Pergamon, 1st Jan. 1970, pp. 716–752. ISBN: 978-0-08-013441-3. DOI: 10.1016/B978-0-08-013441-3.50016-2. URL: https://www.sciencedirect.com/science/article/pii/B9780080134413500162 (visited on 15/09/2021).

[16] K.–S. Choi et al. 'Turbulent Drag Reduction Using Compliant Surfaces'. In: *Proceedings of the Royal Society of London. Series A: Mathematical, Physical and Engineering Sciences* 453.1965 (8th Oct. 1997), pp. 2229–2240. DOI: 10.1098/rspa.1997.0119. URL: https://royalsocietypublishing.org/doi/abs/10.1098/rspa.1997.0119 (visited on 15/09/2021).

[17] Katharina Klausmann and Bodo Ruck. 'Drag Reduction of Circular Cylinders by Porous Coating on the Leeward Side'. In: *Journal of Fluid Mechanics* 813 (25th Feb. 2017), pp. 382–411. ISSN: 0022-1120, 1469-7645. DOI: 10.1017/jfm.2016.757. URL: https://www.cambridge.org/core/product/identifier/S0022112016007576/type/journal_article (visited on 15/09/2021).

[18] Richard Truesdell et al. 'Drag Reduction on a Patterned Superhydrophobic Surface'. In: *Physical Review Letters* 97.4 (26th July 2006), p. 044504. DOI: 10.1103/PhysRevLett.97.044504. URL: https://link.aps.org/doi/10.1103/PhysRevLett.97.044504 (visited on 15/09/2021).

[19] Michael J. Walsh. 'Riblets as a Viscous Drag Reduction Technique'. In: *AIAA Journal* 21.4 (1983), pp. 485–486. ISSN: 0001-1452. DOI: 10.2514/3.60126. URL: https://doi.org/10.2514/3.60126 (visited on 15/09/2021).

[20] Haecheon Choi, Parviz Moin, and John Kim. 'Direct Numerical Simulation of Turbulent Flow over Riblets'. In: *Journal of Fluid Mechanics* 255 (Oct. 1993), pp. 503–539. ISSN: 1469-7645, 0022-1120. DOI: 10.1017/S0022112093002575. URL: https://www.cambridge.org/core/journals/journal-of-fluid-mechanics/article/direct-numerical-simulation-of-turbulent-flow-over-riblets/8A0DAF9111A41A42EF3F401B10C0594C (visited on 15/09/2021).

[21] Ricardo García-Mayoral and Javier Jiménez. 'Drag Reduction by Riblets'. In: *Philosophical Transactions of the Royal Society A: Mathematical, Physical and Engineering Sciences* 369.1940 (13th Apr. 2011), pp. 1412–1427. DOI: 10.1098/rsta.2010.0359. URL: https://royalsocietypublishing.org/doi/full/10.1098/rsta.2010.0359 (visited on 15/09/2021).

[22] Maurizio Quadrio, Pierre Ricco, and Claudio Viotti. 'Streamwise-Travelling Waves of Spanwise Wall Velocity for Turbulent Drag Reduction'. In: *Journal of Fluid Mechanics* 627 (May 2009), pp. 161–178. ISSN: 1469-7645, 0022-1120. DOI: 10.1017/S0022112009006077. URL: https://www.cambridge.org/core/journals/journal-of-fluid-mechanics/article/abs/streamwisetravelling-waves-of-spanwise-wall-velocity-for-turbulent-drag-reduction/17D9C12129254028993F89BD4451C335 (visited on 10/09/2021).

[23] J. R. Debisschop and F. T. M. Nieuwstadt. 'Turbulent Boundary Layer in an Adverse Pressure Gradient - Effectiveness of Riblets'. In: *AIAA Journal* 34.5 (1st May 1996), pp. 932–937. ISSN: 0001-1452. DOI: 10.2514/3.13170. URL: https://arc.aiaa.org/doi/10.2514/3.13170 (visited on 15/09/2021).

[24] E. Coustols and V. Schmitt. 'Synthesis of Experimental Riblet Studies in Transonic Conditions'. In: *Turbulence Control by Passive Means*. Ed. by E. Coustols. Fluid Mechanics and Its Applications. Dordrecht: Springer Netherlands, 1990, pp. 123–140. ISBN: 978-94-009-2159-7. DOI: 10.1007/978-94-009-2159-7_8.

[25] D.W. Bechert and W. Hage. 'Drag Reduction with Riblets in Nature and Engineering'. In: *WIT Transactions on State of the Art in Science and Engineering*. Ed. by R. Liebe. 1st ed. Vol. 2. WIT Press, 10th Nov. 2006, pp. 457–504. ISBN: 978-1-84564-095-8. DOI: 10.2495/1-84564-095-0/5g. URL: http://library.witpress.com/viewpaper.asp?pcode=1845640950-507-1 (visited on 15/09/2021).

[26] J. Szodruch. 'Viscous Drag Reduction on Transport Aircraft'. In: *29th Aerospace Sciences Meeting*. Aerospace Sciences Meetings. American Institute of Aeronautics and Astronautics, 7th Jan. 1991. DOI: 10.2514/6.1991-685. URL: https://arc.aiaa.org/doi/10.2514/6.1991-685 (visited on 15/09/2021).

[27] Shabnam Raayai-Ardakani and Gareth H. McKinley. 'Geometric Optimization of Riblet-Textured Surfaces for Drag Reduction in Laminar Boundary Layer Flows'. In: *Physics of Fluids* 31.5 (May 2019), p. 053601. ISSN: 1070-6631, 1089-7666. DOI: 10.1063/1.5090881. URL: http://aip.scitation.org/doi/10.1063/1.5090881 (visited on 16/09/2021).

[28] Sergei Chernyshenko. *Drag Reduction by a Solid Wall Emulating Spanwise Oscillations. Part 1*. 16th Apr. 2013. arXiv: 1304.4638 [physics.flu-dyn]. URL: http://arxiv.org/abs/1304.4638 (visited on 10/09/2021).

[29] Hermann Schlichting and Klaus Gersten. *Boundary-Layer Theory*. Springer, 2016. ISBN: 3-662-52919-X.

[30] G.E. Karniadakis and Kwing-So Choi. 'Mechanisms on Transverse Motions in Turbulent Wall Flows'. In: *Annual Review of Fluid Mechanics* 35.1 (1st Jan. 2003), pp. 45–62. ISSN: 0066-4189. DOI: 10.1146/annurev.fluid.35.101101.161213. URL: https://doi.org/10.1146/annurev.fluid.35.101101.161213 (visited on 15/09/2021).

[31] M. R. Dhanak and C. Si. 'On Reduction of Turbulent Wall Friction through Spanwise Wall Oscillations'. In: *Journal of Fluid Mechanics* 383 (1999), pp. 175–195. ISSN: 0022-1120. DOI: 10.1017/S0022112098003784. URL: https://www.cambridge.org/core/article/on-reduction-of-turbulent-wall-friction-through-spanwise-wall-oscillations/F524851737C573EFAD0AA19B4AE06CF5 (visited on 16/09/2021).

[32] Arturo Baron and Maurizio Quadrio. 'Turbulent Drag Reduction by Spanwise Wall Oscillations'. In: *Applied Scientific Research* 55.4 (1996), pp. 311–326. ISSN: 0003-6994, 1573-1987. DOI: 10.1007/BF00856638. URL: http://link.springer.com/10.1007/BF00856638 (visited on 15/09/2021).

[33] P. Baj, P. J. K. Bruce, and O. R. H. Buxton. 'The Triple Decomposition of a Fluctuating Velocity Field in a Multiscale Flow'. In: *Physics of Fluids* 27.7 (1st July 2015), p. 075104. ISSN: 1070-6631. DOI: 10.1063/1.4923744. URL: https://aip.scitation.org/doi/10.1063/1.4923744 (visited on 16/09/2021).

[34] Stephen B. Pope. 'Turbulent Flows'. In: *Measurement Science and Technology* 12.11 (Oct. 2001), pp. 2020–2021. ISSN: 0957-0233. DOI: 10.1088/0957-0233/12/11/705. URL: https://doi.org/10.1088/0957-0233/12/11/705 (visited on 17/09/2021).

[35] J. Jeong and F. Hussain. 'On the Identification of a Vortex'. In: *Journal of Fluid Mechanics* 285 (Feb. 1995), pp. 69–94. ISSN: 1469-7645, 0022-1120. DOI: 10.1017/S0022112095000462. URL: https://www.cambridge.org/core/journals/journal-of-fluid-mechanics/article/on-the-identification-of-a-vortex/D26006DDB95FB28DA80E28A581182DF1 (visited on 18/09/2021).

[36] Kwing-So Choi, Timothy Jukes, and Richard Whalley. 'Turbulent Boundary-Layer Control with Plasma Actuators'. In: *Philosophical Transactions of the Royal Society A: Mathematical, Physical and Engineering Sciences* 369.1940 (13th Apr. 2011), pp. 1443–1458. DOI: 10.1098/rsta.2010.0362. URL: https://royalsocietypublishing.org/doi/full/10.1098/rsta.2010.0362 (visited on 18/09/2021).

[37] F. Auteri et al. 'Experimental Assessment of Drag Reduction by Traveling Waves in a Turbulent Pipe Flow'. In: *Physics of Fluids* 22.11 (1st Nov. 2010), p. 115103. ISSN: 1070-6631. DOI: 10.1063/1.3491203. URL: https://aip.scitation.org/doi/full/10.1063/1.3491203 (visited on 18/09/2021).

[38] Maurizio Quadrio and Paolo Luchini. 'Method for Reducing the Viscous Friction between a Fluid and an Object'. Pat. WO2009000703A1 (WO). Politecnico Di Milano, Universita' Degli Studi Di Salerno. 31st Dec. 2008. URL: https://patents.google.com/patent/WO2009000703A1/en?oq=Patent+WO%2f2009%2f000703%2c+2008. (visited on 18/09/2021).

[39] Felix Kramer et al. 'Wavy Riblets for Turbulent Drag Reduction'. In: *5th Flow Control Conference*. 5th Flow Control Conference. Chicago, Illinois: American Institute of Aeronautics and Astronautics, 28th June 2010. ISBN: 978-1-62410-140-3. DOI: 10.2514/6.2010-4583. URL: https://arc.aiaa.org/doi/10.2514/6.2010-4583 (visited on 18/09/2021).

[40] Rene Grüneberger et al. 'Influence of Wave-Like Riblets on Turbulent Friction Drag'. In: *Nature-Inspired Fluid Mechanics: Results of the DFG Priority Programme 1207 "Nature-Inspired Fluid Mechanics" 2006-2012*. Ed. by Cameron Tropea and Horst Bleckmann. Notes on Numerical Fluid Mechanics and Multidisciplinary Design. Berlin, Heidelberg: Springer, 2012, pp. 311–329. ISBN: 978-3-642-28302-4. DOI: 10.1007/978-3-642-28302-4_19. URL: https://doi.org/10.1007/978-3-642-28302-4_19 (visited on 18/09/2021).

[41] Sacha Ghebali, Sergei I. Chernyshenko, and Michael A. Leschziner. 'Can Large-Scale Oblique Undulations on a Solid Wall Reduce the Turbulent Drag?' In: *Physics of Fluids* 29.10 (1st Oct. 2017), p. 105102. ISSN: 1070-6631. DOI: 10.1063/1.5003617. URL: https://doi.org/10.1063/1.5003617 (visited on 10/09/2021).

[42] Sacha Ghebali. 'Turbulent Drag Reduction by Oblique Wavy Wall Undulations'. In: (Apr. 2018). DOI: 10.25560/63827. URL: http://spiral.imperial.ac.uk/handle/10044/1/63827 (visited on 18/09/2021).